Rock and Soil Mechanics

Volume 44 | Issue 4 Article 2

7-19-2023

Penetration resistance evolution characteristics and mesoscopic mechanism of submarine pipeline in sandy seabed

Yang YANG
School of Civil Engineering, Tianjin University, Tianjin 300350, China, State Key Laboratory of Hydraulic Engineering Simulation and Safety, Tianjin University, Tianjin 300350, China

Ying-hui TIAN
School of Engineering, The University of Melbourne, Victoria 3010, Australia

Chun-hui ZHANG
School of Civil Engineering, Hebei University of Science and Technology, Shijiazhuang, Hebei 050018, China

Rong WANG
School of Civil Engineering, Tianjin University, Tianjin 300350, China, State Key Laboratory of Hydraulic Engineering Simulation and Safety, Tianjin University, Tianjin 300350, China

See next page for additional authors

Penetration resistance evolution characteristics and mesoscopic mechanism of submarine pipeline in sandy seabed

Authors

Yang YANG, Ying-hui TIAN, Chun-hui ZHANG, Rong WANG, Zhi-chao WANG, and Le WANG

Rock and Soil Mechanics 2023 44(4): 1001−1008 ISSN 1000−7598
https: //doi.org/10.16285/j.rsm.2022.5755 http://rocksoilmech.researchcommons.org/journal

Penetration resistance evolution characteristics and mesoscopic mechanism of submarine pipeline in sandy seabed

YANG Yang[1, 2], TIAN Ying-hui[3], ZHANG Chun-hui[4], WANG Rong[1, 2], WANG Zhi-chao[5], WANG Le[1, 2]

1. School of Civil Engineering, Tianjin University, Tianjin 300350, China
2. State Key Laboratory of Hydraulic Engineering Simulation and Safety, Tianjin University, Tianjin 300350, China
3. School of Engineering, The University of Melbourne, Victoria 3010, Australia
4. School of Civil Engineering, Hebei University of Science and Technology, Shijiazhuang, Hebei 050018, China
5. School of Civil Engineering, Xiangtan University, Xiangtan, Hunan 411105, China

Abstract: Understanding the vertical penetration process of submarine pipelines is of fundamental significance for the reasonable assessment of the initial pipeline embedment during installation and safety and stability during service. Geotechnical centrifuge model tests, combined with discrete element method modelling were conducted to investigate penetration resistance evolution characteristics and mesoscopic mechanism of submarine pipeline in sand with different densities under the real stress level. The test results show that for the medium-dense sand, the pipe penetration resistance−embedment curve shows a hardening trend. On the other hand, for the dense sand, the pipe penetration resistance−embedment curve exhibits a periodic softening trend; moreover, the deeper the embedment is, the greater the degree of softening becomes. Discrete element modelling results demonstrate that the difference in pipe penetration resistance−embedment curves is induced by different soil movement and failure modes when pipe penetrates in sands with different densities. The pipe penetration resistance evolution characteristics are closely related to the formation and development of shear band in sand. The evolution characteristics of penetration resistance with embedment should be fully considered when evaluating pipe embedment in dense sands using the current design specification for submarine pipelines. More specifically, the pipe embedment should be reasonably estimated based on the upper and lower limits of calculation results, when the preliminarily estimated pipe embedment is larger than one tenth of the pipe diameter.
Keywords: sandy seabed; submarine pipeline; penetration resistance; embedment; discrete element method

1 Introduction

Submarine pipelines are the lifeline of offshore oil and gas transportation, and their safe operation is one of the key technologies in the development of marine oil and gas resources. Deep-sea pipelines are usually laid directly on the seabed and then vertically penetrated to the seabed at a certain depth due to the self-weight and external loads. The pipeline embedment is one of the vital input parameters in the geotechnical engineering design of submarine pipelines, involving many aspects such as as-laid stability, fatigue life, lateral buckling, and axial "walking"[1]. In the pipeline engineering design, it is generally not possible to adopt a conservative value for estimating the pipeline embedment and cannot use conservative extreme estimates, as either overestimation or underestimation of the embedment has adverse effects on the safety and stability of the pipeline. For example, although a great pipeline embedment increases the lateral soil resistance and thus ensuring the pipeline stability, it also reduces the convective heat loss of the pipeline, which leads to the high temperature in the pipeline far from the wellhead and consequently induces thermal expansion[2]. It is crucial to gain a deep understanding of the vertical penetration process of sub-marine pipelines for the reasonable and accurate evaluation of the initial pipeline embedment after installation.

Researchers have conducted extensive studies on the vertical penetration of pipelines in clay. Murff et al.[3], Randolph and White[4] proposed the theoretical solution of undrained vertical bearing capacity in shallowly embedded submarine pipelines in homogeneous clay based on classical plasticity theory. These results have become the theoretical guidance on evaluating the pipeline embedment in the clayey seabed, which are widely used in finite element analysis[5−6] and validated by centrifuge modelling tests[7−8]. There is an increase in demand for submarine pipelines in regions such as the North Sea, Indonesia, the Gulf of Mexico, and the Bohai Sea in China, where the seabed sand is widely distributed in the deep-water environment. Therefore, it is necessary to investigate the vertical penetration of pipelines in sandy soil and provide guidance on evaluating the subsea pipeline embedment in sandy seabed.

The research on the vertical penetration of submarine pipelines in sand is relatively limited. Based on the extensive published experimental results, Verley et al.[9] proposed empirical formulas between pipeline penetration resistance and embedment in silica sand by dimensional and regression analysis. Sandford[10] conducted 1*g* physical model tests on the pipeline vertical penetration in silica sand and found an approximately linear relationship between pipeline

Received: 20 May 2022 Accepted: 9 August 2022
This work was supported by the National Natural Science Foundation of China (51890913, 51879183).
First author: YANG Yang, male, born in 1995, PhD candidate, majoring in marine geotechnical engineering. E-mail: noah_y@tju.edu.cn

penetration resistance and the ratio of pipeline diameter to embedment. Moreover, the vertical penetration mechanism of the pipeline in the uniform silica sand with a given density was investigated via the particle image velocimetry (PIV) technique. However, the 1*g* small-scale physical model test cannot simulate the real stress level in the prototype, which is remarkably related to the strength and stiffness of the tested sand. Thus, it is difficult to accurately simulate the macroscopic mechanical response of the soil, e.g., the deformation and failure, during the vertical penetration of the pipeline.

The penetration mechanism of pipeline in sandy soils is influenced by soil density, shear dilatancy, internal friction angle, etc., and more complicated than that in clay soils. Due to this reason, thus it is difficult to establish analytical solutions corresponding to that mechanism. For industrial practice, there is still significant uncertainty over evaluating pipeline embedment in sandy seabed. To gain a better understanding of the vertical penetration process of submarine pipelines in sandy seabed, the geotechnical centrifuge model tests and numerical modeling using discrete elements method on the evolution and mesoscopic mechanism of the vertical penetration resistance of submarine pipelines in sands with different densities have been conducted in the present study.

2 Geotechnical centrifuge model test

The geotechnical centrifuge model tests were performed at the Centre for Offshore Foundation Systems (COFS) at University of Western Australia. The beam geotechnical centrifuge used in this study has a diameter of 3.6 m and a capacity of 40*g*-tonnes at accelerations up to 200*g*. The centrifugal acceleration for this study is 25g.

2.1 Model pipeline and experimental setup

The aluminum model pipeline had a length (L) of 120 mm and a diameter (D) of 20 mm, as shown in Fig. 1(a). At a centrifugal acceleration of 25*g*, the model pipeline corresponds to a prototype pipeline with a length of 3 m and a diameter of 0.5 m. The S-type load cell was rigidly connected to the upper surface of the pipeline using threads and was fixed to the loading arm. The lower surface of the pipeline remained cylindrical. As shown in Fig. 1(b), the S-type load cell had a capacity of 1.8 kN and was used to accurately measure the vertical force acting on the pipeline. The diameter at the end section of the loading arm was 12 mm, as shown in Fig. 1(c).

2.2 Tested soil and specimen preparation

The silica fine sand was used in this study. The soil particles are dominated with sub-rounded and sub-angular shapes. The main mineralogical composition was silicon dioxide (SiO_2). The specific gravity (G_s) was 2.65. The maximum dry density (ρ_{max}) was 1 774 kg /m^3, and the minimum dry density (ρ_{min}) was 1 497 kg /m^3. The median particle size (d_{50}) was 0.17 mm. The coefficient of uniformity (C_u) was 1.67, and the coefficient of curvature (C_c) was 1.02. The critical internal friction angle of the sand (φ_c) was 33º. Figure 2 shows the particle size distribution curve of the silica fine sand. According to the studies by Ovesen[11], the effect of particle size on the model test results was negligible when the ratio of the pipeline diameter to the median sand particle size D/d_{50} was greater than 30. In this study, D/d_{50} was 120 and much greater than 30; therefore, the effect of particle size can be neglected.

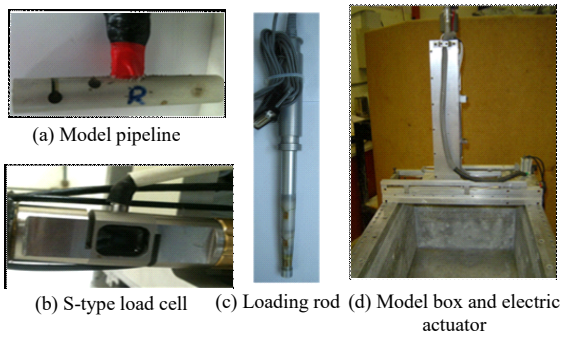

Fig. 1 Pipe model and model test configuration

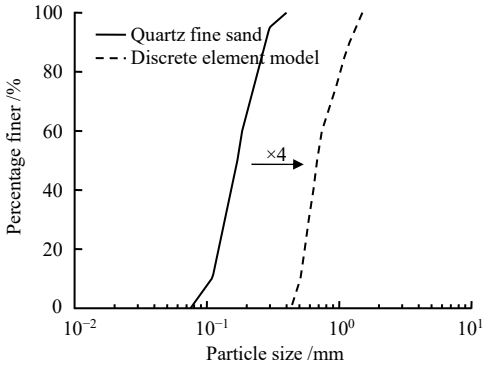

Fig. 2 Particle size distribution curves

The internal dimensions of the model box are 650 mm (length)×390 mm (width)×325 mm (height), as shown in Fig. 1(d). To simulate the formation of natural sandy seabed and ensure the repeatability and uniformity of the soil specimen, two boxes of soil specimens were prepared using pluviation. One specimen was placed on a vibration table and vibrated for 2 minutes to prepare a dense soil specimen labeled as “SD”; the other one was not vibrated to prepare a medium-dense soil specimen labeled as “SM”. The surface of soil specimens was scraped off to obtain a flat surface. The density of the soil specimen was calculated after the preparation, which was listed in Table 1. As the permeability of the sandy soil was high, the soil was in a completely drained state during static penetration of the pipeline. In addition, the degree of saturation has little influence on the drained strength of sandy soils. Thus, the tests were conducted in dry sandy soils, according to previous experimental studies on pipe−soil interaction[10−15].

2.3 Cone penetration test

To exam the uniformity of the prepared soil specimens, the cone penetration test (CPT) was performed prior to the vertical penetration of the pipeline under the same

Table 1 Details of tested sand specimens

No.	Dry density ρ/(kg • m^{-3})	Relative density D_r/%	State[12]	Internal friction angle φ/(°)
SM	1 626	50	Medium-dense	36.2
SD	1 702	77	Dense	38

conditions of a centrifugal acceleration of 25*g*. Figure 3 shows the cone resistance versus depth profiles for two soil specimens. The horizontal axis represents the cone resistance q_c, and the vertical one represents the normalized depth, z/D (z is the cone penetration depth, and D is the pipeline diameter). It can be found that the cone resistance increases linearly with the normalized depth, which indicates a good uniformity of the prepared specimen. Moreover, the greater the soil density is, the greater the cone resistance is at a given depth, which indicates that the prepared specimens meet the requirements of different degrees of compaction in this study.

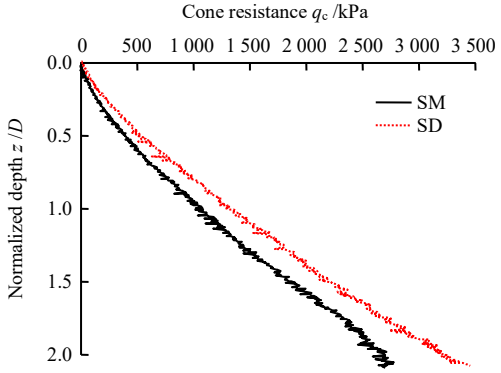

Fig. 3 Profiles of cone tip resistances for sand specimens SM and SD

2.4 Loading method and data acquisition

As shown in Fig. 1(d), an electric actuator was used for loading. The actuator is driven by a DC servo motor, which had a maximum vertical load of 8 kN and a maximum vertical displacement of 240 mm. In this study, displacement loading method was used. As shown in Fig. 4, the pipeline was vertically penetrated to the depth of one half of the pipeline diameter, i.e., 0.5D at a constant velocity of 1 mm /s. Typically, the embedment of a thermally insulated seabed pipeline in engineering practice is smaller than 0.5D[2]. The high-speed wireless data acquisition system (WDAS) in-house developed at University of Western Australia was used for data acquisition and system control. Real-time coordination was achieved between the system control by the actuator and data transmission. The data acquisition frequency was 10 Hz.

Fig. 4 Pipe penetration process

3 Test results and analysis

Figure 5 shows the measured penetration resistance–embedment profiles (model dimensions have been converted to prototype dimensions). The horizontal axis represents the pipeline penetration resistance per unit length, V; and the vertical one stands for the normalized embedment w/D, where w is the embedment of the pipeline. Figure 5 also includes the estimated results for comparison in accordance with the code DNVGL-RP-F114[16]. As shown in Fig. 5(a), for the medium-dense soil specimen SM, when w is smaller than 0.05D, the penetration resistance increases rapidly to 50 kN /m with the increase in pipeline embedment; when w ranges from 0.05D to 0.15D, the penetration resistance remains nearly unchanged; when w increases from 0.15D to 0.4D, the penetration resistance continues to increase and gradually stabilizes; and when w is greater than 0.4D, the penetration resistance increases again until the end of the test. It can be found that the pipeline penetration resistance–embedment profile in the SM soil exhibits the hardening characteristics, which is approximately consistent with the upper bound values calculated according to the code DNVGL-RP-F114.

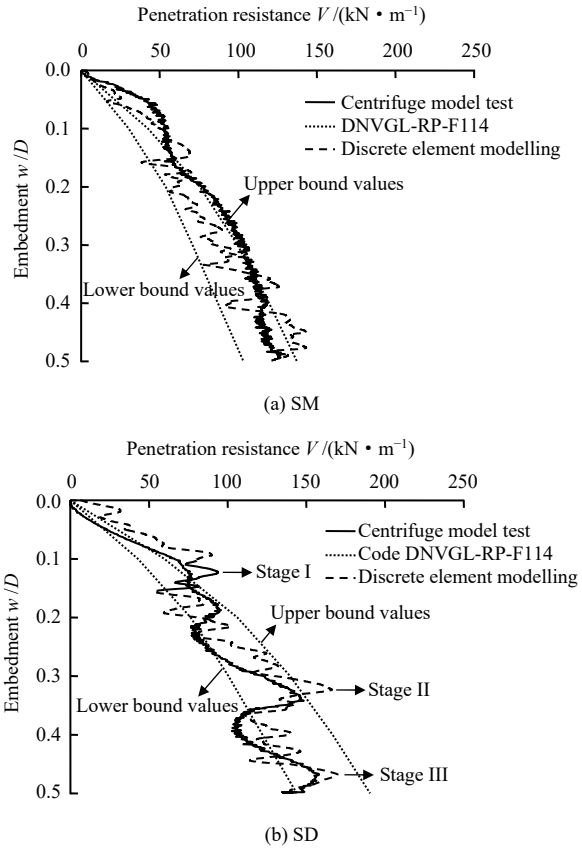

Fig. 5 Penetration resistance–embedment curves

As shown in Fig. 5(b), for the dense soil specimen SD, when w is smaller than 0.1D, the penetration resistance increases linearly to 75 kN /m with the embedment, which is very close to the upper bound value calculated according to the code DNVGL-RF-114; when w increases from 0.1D to 0.2D, the penetration resistance generally shows an increasing trend, which has several drops to different extent and fluctuates between the upper and lower bound values calculated according to the code; when w reaches about 0.2D, the penetration resistance decreases from 100 kN /m to 75 kN /m; when w ranges from 0.35D to 0.4D, the penetration resistance decreases from 150 kN /m to 100 kN /m; and when w is greater than 0.45D, the penetration resistance decreases again from 150 kN /m until the end of the test. It can be found that the amplitude of the decrease in penetration resistance gradually increases with increasing embedment in the soil SD. In addition, the penetration resistance− embedment profile in the SD soil shows a periodic softening feature.

The comparison between Figs. 5(a) and 5(b) indicates that there is not a remarkable increase in the penetration resistance as the soil density increases. For example, when w is 0.5D, the penetration resistance of the medium-dense soil specimen SM is 125 kN /m, while the penetration resistance of the dense soil specimen SD is only 150 kN /m. Even in some cases, the penetration resistance of the dense soil specimen SD is smaller than that of the medium-dense soil specimen SM. For instance, when w is 0.4D, the penetration resistance of the medium-dense soil specimen SM is 120 kN /m, while the penetration resistance of the dense soil specimen SD is 106 kN /m.

The centrifuge model test results indicate that the soil density significantly influences the evolution characteristics of the vertical penetration resistance for pipelines in sands. To investigate the reason for this phenomenon, the numerical modelling of the vertical penetration process of the pipeline in sands will be conducted in the next section. The meso-mechanism on the evolution characteristics of the pipeline vertical penetration resistance in sands with different densities will be addressed as well.

4 Mesoscopic mechanism investigation

The discrete element method can effectively simulate the change in mesostructure and particle-level properties of granular materials under discontinuous or large deformation conditions. In this study, the two-dimensional discrete element method was used to investigate the mesoscopic penetration mechanism of the pipeline in sands with different densities.

4.1 Establishment of discrete element model

Figure 6 illustrates the discrete element numerical model. As shown in Fig. 6, the two-dimensional plane strain model has the dimensions of 13D (width W)×5.5D (height H). The diameter of the pipeline model (D) is 20 mm, which is the same as the size of the pipeline model in the centrifuge model tests. In order to improve the efficiency of the simulation and capture the change in the mesostructure inside the sand during the pipeline penetration, the particle size of the model is 4 times the size of real sand particle as shown in Fig. 2. In the numerical soil model, the median particle size (d_{50}) is 0.68 mm, and the maximum void ratio (e_{max}) and minimum void ratio (e_{min}) are 0.275 and 0.175, respectively. Table 2 summarizes the information on the model and particle size used for discrete element modelling in the existing studies on the pipe−soil interaction. It can be found that the dimensions of the model in this study, i.e., W/D = 13 and D/d_{50} = 29.4, is the maximum compared with the reported two-dimensional discrete element models on shallowly embedded pipelines. The boundary effect and the particle size effect can be negligible when $W/D \geqslant 2.82$ and $D/d_{50} > 30$, based on the studies by Ovesen[11]. The numerical model in this study meets those requirements, therefore the boundary effect and the particle size effect can be neglected. The mesoscopic parameters of the numerical model are listed in Table 3.

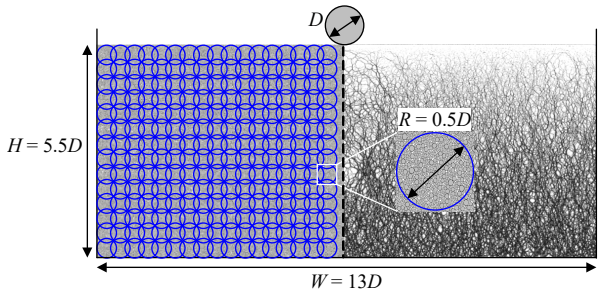

Fig. 6 Schematic diagram of discrete element model

Table 2 Parameters of DEM modelling for pipe−soil interaction in existing literatures and the present study

Sources	Type	Dimension	W/D	D/d_{50}
Calvetti et al.[17]	Deeply embedded	3D	16	2.5
Yimsiri et al.[18]	Deeply embedded	3D	~19	1.6, 4.8
Jiang et al.[19]	Deeply embedded	2D	16	~7.9
Macaro[20]	Shallowly embedded	3D	5, 7	~15.6, ~31.2
Zhao et al.[21]	Shallowly embedded	2D	12	18
This study	Shallowly embedded	2D	13	29.4

Note: "~" stands for "around".

The soil specimen in this discrete element modelling study was generated by the multi-layer with undercompaction method[22]. After the soil specimen generation was completed, gravitational acceleration of 1g was applied to the soil sample and the calculation was cycled until equilibrium, simulating 1g of sample preparing conditions in laboratory. Subsequently, a centrifugal acceleration of 25g was applied and the soil specimen arrived at a new equilibrium after the iterated calculation, which simulated the condition of the centrifugal acceleration of 25g in the geotechnical centrifuge model test. Two boxes of soil specimens were generated with the relative densities of D_r = 48% (i.e., void ratio e = 0.227) and D_r =

78% (i.e., void ratio e = 0.197), which were close to those in the centrifuge model tests. The total numbers of soil particles were 58710 and 60150 for SM and SD, respectively.

Table 3 Mesoscopic parameters of DEM model in the present study

	Mesoscopic parameters	Value
Soil	Normal stiffness k_n /(N • m^{-1})	7.5×10^7
	Tangential contact stiffness k_s /(N • m^{-1})	5×10^7
	Coefficient of friction μ	0.4
	Coefficient of rolling resistance μ_r	0.8
	Coefficient of damping D	0.7
Pipeline	Normal stiffness k_n /(N • m^{-1})	1×10^9
	Tangential contact stiffness k_s /(N • m^{-1})	1×10^9
	Coefficient of friction μ	0.3
Wall	Normal stiffness k_n /(N • m^{-1})	1×10^9
	Tangential contact stiffness k_s /(N • m^{-1})	1×10^9
	Coefficient of friction μ	0

To monitor the change of the mesostructure inside the soil specimen, a series of measuring circles with a diameter of 0.5D was arranged as shown in the left of Fig. 6. Each measuring circle contains at least 200 particles, which ensures the accuracy of the measured results[22]. Figure 7 shows the variations of porosity n, horizontal stress σ_h, vertical stress σ_v, and lateral earth pressure coefficient K_0 with respect to depth at the initial state of the soil specimens. The porosity n of the soil specimen remains almost unchanged with respect to the depth, which indicates the uniformity of the prepared soil specimen. The σ_h and σ_v increase linearly as the depth increases. The K_0 decreases and then levels off with increasing depth. This may be induced by the multi-layer with undercompaction method, which compacting the soil specimen within a certain depth range to a desired void ratio. The compaction energy is transferred to the layers below except for the last layer, which results in the relatively greater disturbance in the upper layers[22]. The K_0 of the SM is greater than that of the SD, which indicates the soil specimen is more isotropic when the soil density is lower.

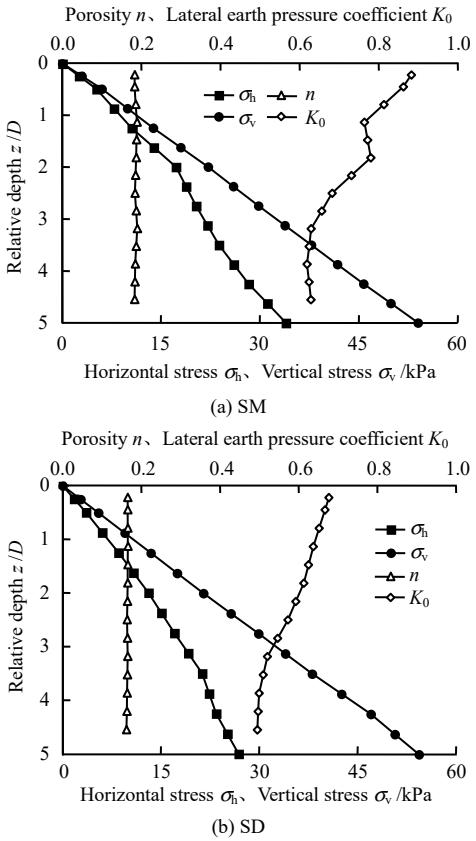

Fig. 7 Variations of porosity, horizontal and vertical stresses, and lateral earth pressure coefficient with the relative depth

Typically, the vertical penetration of the pipeline in the sand is a quasi-static process. If the penetration velocity in the numerical modelling is the same as that in the centrifuge model test, the computational cost will remarkably increase. If an extremely high penetration velocity for the numerical modelling is used, the intensive particle overlapping will occur in a short duration after loading. Moreover, the dynamic effect will result in distorted results. According to the studies by Tran et al.[23], the dynamic effect during the penetration process can be quantified by the inertial parameter I:

$$I = \dot{\gamma}\sqrt{\frac{m}{P}} \tag{1}$$

$$\dot{\gamma} = \frac{v}{H} \tag{2}$$

where $\dot{\gamma}$ is the strain rate; m is the particle mass; P is the overburden pressure; and v is the penetration velocity. Typically, when the inertial parameter I is not greater than 10^{-3}, the quasi-static loading condition can be assumed. To improve the computational efficiency and to ensure the numerical accuracy, the penetration velocity v = 0.01 m /s is used in this study. According to Eqs. (1) and (2), the estimated inertial parameter $I = 4.38\times10^{-4}$, which meets the requirement for the quasi-static loading condition.

4.2 Validation of numerical model

Figure 5 presents the discrete element modelling results on the penetration resistance−embedment profiles during the vertical penetration process of the pipeline, which are compared with the centrifuge model test results. It can be seen that the discrete element modelling results are generally consistent with the centrifuge model test results. For the SM, the penetration resistance gradually increases with increasing depth. For the SD, the penetration resistance has several drops to different extent at depths of (0.1−0.2)D (i.e., stage I), (0.3−0.4)D (i.e., stage II), and (0.4−0.5)D (i.e., stage III). It should be noted that although the discrete element modelling results have the discrepancies with the model test results, which are affected by the number and shape of particles in the model, the overall evolution characteristics of the pipeline penetration resistance in sand specimens with different

densities are similar to those obtained from the centrifuge model tests.

4.3 Numerical modelling results and analysis

4.3.1 Deformation and failure mode of soil

Figure 8 gives the soil surface change at the end of the pipeline penetration. Soil heave occurs on both sides of the pipeline. As shown in Fig. 8, for the SM, the height of soil heave h is about 0.15D; for the SD, h is about 0.25D. The range where the heave occurs on the soil heave l is approximate the same for both specimens and is about 2D. It can be found that the higher the density of the soil specimen is, the more significant soil heave is generated after the pipeline penetration.

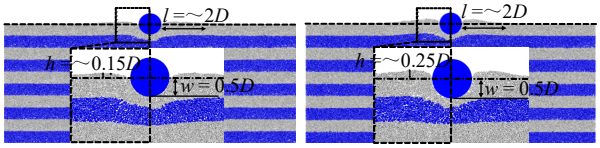

(a) SM (b) SD

Fig. 8 Movement of sand ground surface

Figure 9 shows the velocity field of sand particles during the vertical penetration of the pipeline. The embedment w = 0.5D is presented for illustration, where the dashed line approximately distinguishes the flow region and the non-flow region in the soil specimen, and the darker color represents a greater velocity of the sand particle. It can be seen that the flow velocity of sand particles at the bottom of the pipeline has the same magnitude, i.e., 0.01 m /s and different directions in soil specimen with different densities. As shown in Fig. 9(a), for the SM, the soil at the bottom of the pipeline mainly flows to the lower left with non-symmetric local flow towards both sides, which indicates the failure mode transits from punching shear to local shear failure. As shown in Fig. 9(b), for the SD, it can be observed that the soil at the bottom of the pipeline flows in a wedge shape towards the ground surface on both sides of the pipeline and the deep soil almost remains undisturbed, which suggests a typical shallow general shear failure mode.

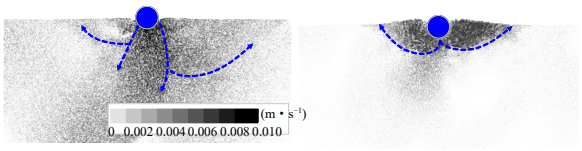

(a) SM (b) SD

Fig. 9 Velocity field of sand particles

4.3.2 Formation and development of shear band

Figure 10 shows the particle rotation field during the vertical penetration of the pipeline at the embedment of 0.1D, 0.2D, 0.3D, 0.4D, and 0.5D. The red color indicates that the counterclockwise rotation is greater than 20°; while the green color indicates that clockwise rotation is greater than 20°. It can be observed that at the beginning of the pipeline penetration, sand particles with the remarkable rotation and opposite directions appear first on both sides of the bottom of the pipeline. As the embedment increases, sand particles with the remarkable rotation are concentrated on the shear bands, and the particles on each shear band have the same rotation direction.

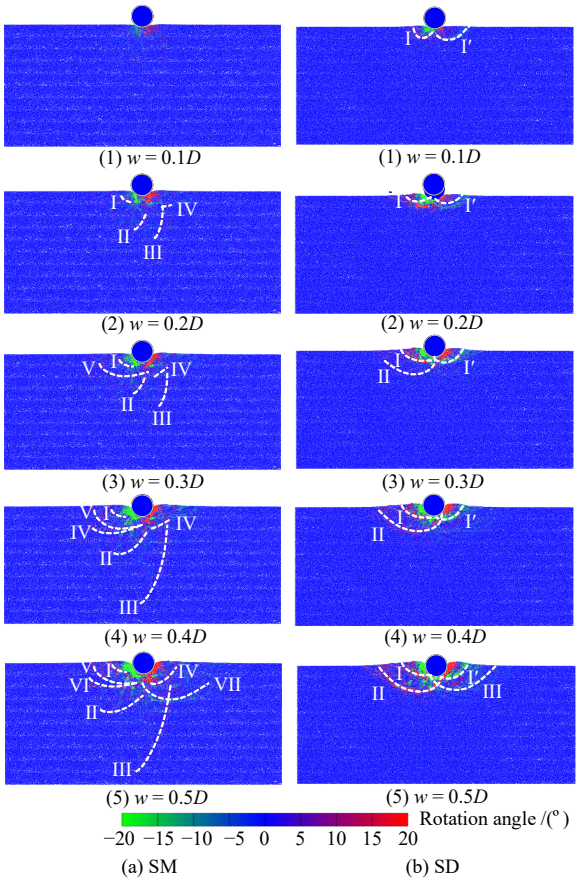

(a) SM (b) SD

Fig. 10 Rotation field of sand particles

Figure 10(a) shows the rotation field of sand particles during the vertical penetration of the pipeline in the SM. Several shear bands with different lengths form inside the soil during the pipeline penetration process. When w = 0.2D, as shown in Fig. 10(a), shear bands I–IV form and the penetration resistance is almost stable. When w = 0.3D, the shear band V appears but shear bands I–IV stop developing, and the penetration resistance increases slowly. When w = 0.4D, the shear band VI starts to form, and shear bands II and III continue to extend towards the bottom, and the penetration resistance remains basically unchanged. When w = 0.5D, the shear band VII starts to form and extends to the ground surface, while the other shear bands and the penetration resistance remain almost unchanged. For the SM, although multiple shear bands form during the pipeline penetration, most of the shear bands do not extend to the ground surface. The shear bands extend inside the soil and induce the local shear failure, which suggests a slow increase in the penetration resistance as the embedment increases from a macroscopic point of view.

Figure 10(b) shows the rotation field of sand particles

during the vertical penetration of the pipeline in SD. Multiple shear bands extend to the ground surface on both sides of the pipeline during the penetration process. When $w = 0.1D$, as shown in Fig. 10(b), shear bands I and I′ form on both sides of the bottom of the pipeline, accompanied by a slight decrease in the penetration resistance in stage I as shown in Fig. 5(b). When $w = 0.3D$, a larger shear band II appears on the lower left side of the pipeline, and the penetration resistance decreases significantly in stage II as shown in Fig. 5(b). During the vertical penetration of the pipeline, the penetration resistance approximately equals the sum of the shear strength provided by the soil on the shear band and the vertical component of the weight of the soil wedge. Because the size of shear band II is much larger than that of shear bands I and I′, the shear resistance on the shear band loses when the shear band II extends to the ground surface. Consequently, the soil bearing capacity decreases, which induces the more remarkable decrease in the penetration resistance. Since the failure zone formed by shear band II is larger, the bearing capacity provided by the soil weight is greater. Therefore, the residual penetration resistance after stage II is still greater than the residual penetration resistance after stage I, although the penetration resistance drops to a larger extent during stage II. When $w = 0.5D$, as shown in Fig. 10(b), a shear band III with the approximately same size as shear band II appears on the lower right side of the pipeline, which results in a decrease in the penetration resistance in stage III as shown in Fig. 5(b). It suggests that the decrease in penetration resistance during the pipeline penetration in dense sand is due to the general shear failure associated with the extension of shear bands through the ground surface.

4.3.3 Mesoscopic mechanism for force transmission

Force chains are paths along which inter-particle contact forces are transmitted through the contact network in discrete element models. The evolution of the force-chain distribution qualitatively provides the insight on the mesoscopic mechanism of force transmission during the pipeline penetration. Figure 11 presents the force-chain distribution at the pipeline penetration embedment of $0.1D$, $0.2D$, $0.3D$, $0.4D$, and $0.5D$. The thickness of the force chain represents the magnitude of the contact force. To make it clear, only strong force chains with a magnitude greater than 200 N are plotted in Fig. 11. The comparison between Figs. 11(a) and 11(b) suggests that the distribution range of strong force chains in the SM is larger, and those in the SD are more concentrated. The sand particles have a lower coordination number in the medium-dense soil as compared with the dense soil, which leads the medium-dense soil more susceptible to the stress concentration.

As shown in Fig. 11(a), for the SM, the concentration of strong force chains at the bottom of the pipeline gradually increases, and their distribution range extends downwards to the bottom on both sides with increasing embedment, which indicates that the pipeline penetration resistance mainly comes from the deep soils underneath the pipeline. For the SD, as shown in Fig. 11(b), during the vertical penetration of the pipeline, the strong force chains are densely distributed underneath the pipeline. As the embedment increases, the strong force chains begin to extend towards the both sides of the pipeline at shallow depths. It is similar to the development of shear bands as shown in Fig. 10(b), which indicates that the pipeline penetration resistance originates from the shallow soils on both sides of the pipeline. From Fig. 11(b), it can also be found that the concentration of strong force chains at the bottom of the pipeline periodically decreases as the embedment increases. As shown in red circles in Fig. 11(b), when the embedment arrives at $0.2D$, $0.4D$ and $0.5D$, the strong force chains on both sides of the bottom of the pipeline undergo rupture to different extend compared with the previous stage in the same area. This phenomenon is particularly significant at $w = 0.4D$ as shown in Fig. 11(b). The concentration of strong force chains in the circle at $w = 0.4D$ is more sparse than that at $w = 0.3D$. Thus, the pipeline penetration resistance undergoes a significant decrease from the macroscopic point of view, as shown in stage II in Fig. 5(b).

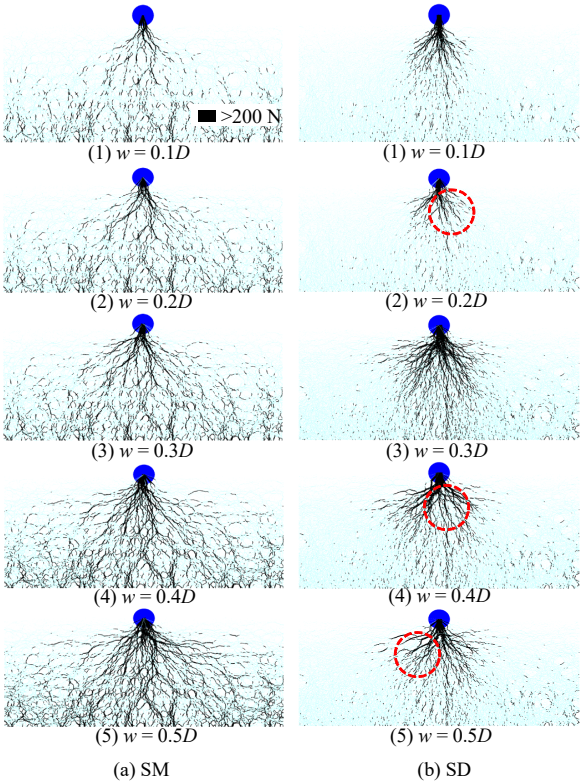

Fig. 11 Distribution characteristics of contact force chains

5 Conclusions

The geotechnical centrifuge model tests, combined with the discrete element modelling have been performed to investigate the evolution characteristics and meso-mechanism of the vertical penetration resistance of submarine pipelines in sands with different densities. The main conclusions are summarized as follows:

(1) The sand density has a significant impact on the evolution of vertical penetration resistance during the

pipeline penetration. For the medium-dense sand, the pipeline penetration resistance−embedment profile mainly exhibits a hardening characteristic. For the dense sand, on the other hand, the pipeline penetration resistance−embedment profile shows a periodic softening characteristic when the pipeline embedment is greater than 0.1*D*. Moreover, the greater the embedment is, the more significant the softening is. When the pipeline embedment is 0.5*D*, the pipeline penetration resistance is approximately 125 kN /m and 150 kN /m for the medium-dense and dense soil specimens, respectively.

(2) The failure mode of the soil during pipeline penetration varies with the sand density. For the medium-dense sand, it suggests a failure mode transition from punching shear failure to local shear failure. For the dense sand, it exhibits the mode of general shear failure. The heave of the ground surface induce by the pipeline penetration has a height of approximately 0.25*D* for the dense sand and 0.15*D* for the medium-dense sand. The influence range of the heave is approximately the same for two soil densities and is around 2*D*.

(3) The evolution of the pipeline penetration resistance is closely related to the formation and development of the shear band. When the extension of the shear band in the soil leads to a local shear failure, the growth rate of the penetration resistance becomes slow during the vertical penetration of the pipeline. When the shear band extends and the general shear failure takes place, the penetration resistance decreases. The larger the size of the shear band is, the more significant the pipeline penetration resistance decreases.

(4) The distribution characteristics of contact force chains indicate that for the medium-dense sand, the pipeline penetration resistance mainly comes from the deep soil on both sides beneath the pipeline; while for the dense sand, the pipeline penetration resistance comes from the shallow soil on both sides of the pipeline.

(5) When evaluating the embedment of the submarine pipeline in dense sands using the current codes for submarine pipelines, the evolution characteristics of penetration resistance with embedment should be considered. When the preliminary estimation of pipeline embedment is greater than 0.1*D*, a reasonable prediction of pipeline embedment can be obtained by accounting for the calculated upper and lower bound results according to the codes.

References

[1] BRUTON D A S, WHITE D J, CHEUK C Y, et al. Pipe-soil interaction behaviour during lateral buckling, including large amplitude cyclic displacement tests by the Safebuck JIP[C]//Proceedings of Offshore Technology Conference. Houston: [s. n.], 2006.

[2] RANDOLPH M, GOURVENEC S. Offshore geotechnical engineering[M]. Abingdon, Oxon, UK: Spon Press, 2011.

[3] MURFF J D, WAGNER D A, RANDOLPH M F. Pipe penetration in cohesive soil[J]. Géotechnique, 1989, 39(2): 213−229.

[4] RANDOLPH M F, WHITE D J. Upper-bound yield envelopes for pipelines at shallow embedment in clay[J]. Géotechnique, 2008, 58(4): 297−301.

[5] MERIFIELD R, WHITE D J, RANDOLPH M F. Analysis of the undrained breakout resistance of partially embedded pipelines[J]. Géotechnique, 2008, 58(6): 461−470.

[6] CHATTERJEE S, RANDOLPH M F, WHITE D J. Numerical simulations of pipe-soil interaction during large lateral movements on clay[J]. Géotechnique, 2012, 62(8): 693−705.

[7] DINGLE H R C, WHITE D J, GAUDIN C. Mechanisms of pipe embedment and lateral breakout on soft clay[J]. Canadian Geotechnical Journal, 2008, 45(5): 636−652.

[8] HODDER M S, CASSIDY M J. A plasticity model for predicting the vertical and lateral behaviour of pipelines in clay soils[J]. Géotechnique, 2010, 60(4): 247−263.

[9] VERLEY R L P, SOTBERY T. A soil resistance model for pipelines placed on sandy soils[J]. Journal of Offshore Mechanics and Arctic Engineering, 1994, 116(3): 145−153.

[10] SANDFORD R J. Lateral buckling of high pressure/high temperature on-bottom pipelines[D]. Oxford, UK: University of Oxford, 2012.

[11] OVESEN N K. The use of physical models in design: the scaling law relationships[C]//Proceedings of the Seventh European Conference on Soil Mechanics and Foundation Engineering. Brighton, United Kingdom: [s. n.], 1979: 318−323.

[12] Ministry of Water Resources of the People's Republic of China. GB/T50123−2019 Standard for geotechnical testing methods[S]. Beijing: China Planning Press, 2019.

[13] WANG L, LIU R. The effect of a berm on the lateral resistance of a shallow pipeline buried in sand[J]. Ocean Engineering, 2016, 121: 13−23.

[14] WANG Z, TANG Y, FENG H, et al. Model test for lateral soil resistance of partially embedded subsea pipelines on sand during large-amplitude lateral movement[J]. Journal of Coastal Research, 2017, 33(3): 607−618.

[15] WANG Yu-fei, LIU Run. Study on vertical-horizontal failure envelopes of shallow-embedded pipelines on sand[J]. Rock and Soil Mechanics, 2019, 40(3): 1129−1139.

[16] DNV G L. DNVGL-RP-F114: Pipe-soil interaction for submarine pipelines[S]. [S. l.]: Recommended Practice, 2017.

[17] CALVETTI F, DI PRISCO C, NOVA R. Experimental and numerical analysis of soil-pipe interaction[J]. Journal of Geotechnical and Geoenvironmental Engineering, 2004, 130(12): 1292−1299.

[18] YIMSIRI S, SOGA K, YOSHIZAKI K, et al. Lateral and upward soil pipeline interactions in sand for deep embedment conditions[J]. Journal of Geotechnical and Geoenvironmental Engineering, 2004, 130(8): 830−842.

[19] JIANG M, ZHANG W, WANG J. DEM analyses of uplift failure mechanism with pipe buried in a cemented granular ground[J]. International Journal of Geomechanics, 2014, 15(5): 04014083.

[20] MACARO G. Distinct element modelling of pipe–soil interaction for offshore pipelines on granular soils[D]. Oxford, UK: University of Oxford, 2015.

[21] ZHAO X, LUAN Y, ZHANG C, et al. Experimental and numerical study of pipelines shallowly embedded in sands[C]// Offshore Site Investigation Geotechnics 8th International Conference Proceeding. [S. l.]: [s. n.], 2017.

[22] JIANG M, KONRAD J M, LEROUEIL S. An efficient technique for generating homogeneous specimens for dem studies[J]. Computers and Geotechnics, 2003, 30(7): 579−597.

[23] TRAN Q A, CHEVALIER B, BREUL P. Discrete modeling of penetration tests in constant velocity and impact conditions[J]. Computers and Geotechnics, 2016, 71: 12−18.